JOURNAL OF COMPUTATIONAL PHYSICS 58, 229–245 (1985)

Conformal-Mapping-Based Coordinate Generation Method for Channel Flows

J. M. FLORYAN

Faculty of Engineering Science, The University of Western Ontario, London, Ontario N6A 5B9, Canada

Received November 29, 1983

A conformal-mapping-based coordinate generation method for channel-type configurations has been developed. A channel of an arbitrary shape in the physical plane is mapped into a straight channel in the computational plane. The parameters of the transformation have to be determined through a method of successive approximations. A simple iteration scheme, that converges quite rapidly even with a poor initial guess, is presented. Solutions for different configurations are displayed to illustrate the capabilities of the method. Results of the tests show higher-order accuracy of the method in the case of curved channels. © 1985 Academic Press, Inc.

1. INTRODUCTION

The common goal of different grid generation procedures is to construct boundary-fitted coordinates. Such coordinates permit writing of general codes that may treat field equations in domains of arbitrary shapes. Grid generation for arbitrary domains has to be done numerically, since analytical solutions exist for only a limited class of geometrical configurations. The wide variety of available methods has been reviewed in the recent papers by Thompson [11] and Thompson and Warsi [12]. The generated coordinates are, in general, curvilinear. The form of the field equations is considerably simplified if the coordinates satisfy the condition of orthogonality. When the coordinates are also conformal, additional simplifications result from the application of the Cauchy–Riemann relations. The major advantage in selecting conformal coordinates is in the fact that their properties are described in terms of only one metric coefficient.

Methods based on conformal mapping have long been utilized to generate coordinate system about curves that are the contours of the mapping. Ives [4] discussed the foundations and implementation of conformal mapping to the grid generation, while Thompson and Warsi [12] provided an extensive review of the existing solutions. Kober [6] gave a list of elementary functions that may be utilized for the mapping purposes. Davis [3] utilized the Schwarz–Christoffel transformation and made a very powerful grid generation tool out of it by extending the transformation to the case of curved contours. Ives [4] discussed extensions of the conformal mapping to a certain class of three-dimensional configurations. The available methods are quite powerful, however, a good understanding of the theory of functions of

0021-9991/85 $3.00
Copyright © 1985 by Academic Press, Inc.
All rights of reproduction in any form reserved.

complex variable may be necessary for their effective application. The most pronounced difficulties are due to the multivaluedness of the transformations and special care is required for the numerical selection of the appropriate Riemann sheet.

Coordinate generation methods for internal flows have been discussed by Knight [5]. O'Brien [7] presented several functions that generate symmetric ductlike configurations. Sridhar and Davis [10] developed a mapping that permitted coordinate fitting for a more general class of duct shapes. This technique has been successfully utilized by Anderson *et al.* [1] for the solution of viscous flow problems. There are several other solutions available for channel configurations [11, 12], however, no mapping with provision for fitting an arbitrary duct has yet been developed.

This paper describes a conformal-transformation-based method of coordinate generation for channels of arbitrary shape. The basic idea of the solution is to map the channel of a given shape in the physical plane into a straight channel in the computational plane. Thus, the solution of the flow problem may be carried in the computational plane with the help of a simple rectangular grid. Transformations being presented are of the Schwarz–Christoffel type and have a semi-analytic form; that is, the form of the transforming function is known, however, its parameters are not. Transformation dealing with a channel bounded by straight wall elements is described in Section 2. The transformation involves parameters defined in the computational plane, and thus not known a priori for the configuration of interest in the physical plane. Section 2.1 gives a description of the numerical procedure permitting determination of the required parameters. This procedure, which involves integration of the mapping function, is $\Delta w^{1.43}$ accurate, where Δw is the integration step, has a simple logic and is easy to program. The difficulties associated with the singularities of the mapping are removed by applying integration procedures described in Section 2.1.2. Section 3 describes the extension of the mapping to the general case, i.e., the case of a channel bounded by straight and curved wall elements. Again, certain parameters of the transformation are defined in the computational plane and therefore are not known a priori for the configuration of interest. The appropriate numerical procedure is described in Section 3.1 and is $\Delta w^{3.49}$ accurate. The mapping described in Sections 2 and 3 can be used to generate coordinates that are not necessarily conformal. Section 4 describes metric coefficients for a conformal system and discusses extension to the axisymmetric and three-dimensional cases. Determination of the parameters of the transformation is equivalent to the solution of the potential flow problem in the channel. Section 5 describes such solutions for several different flow conditions. Streamlines of the inviscid flow behave as optimal coordinates in boundary-layer analysis [13], and therefore, the coordinates described in this paper are particularly well suited for the incorporation of the scaling typical for the high Reynolds number flows.

2. Channels Bounded by Straight Wall Segments

An arbitrary channel, bounded by the straight wall segments in the physical plane, is mapped into a straight channel in the computational plane. The transformation is illustrated in Fig. 1. The individual mappings have the form

$$w = \frac{h}{\pi} \ln t; \qquad \frac{dz}{dt} = Mt^{-1-\delta} \prod_{j=1}^{j=n} (t - c_j)^{\alpha_j}, \tag{1}$$

where M is a complex constant, n determines number of corners, and $\alpha\pi$ denotes corner turning angles. Angles $\alpha\pi$ are taken to be positive for the clockwise rotation when the channel is circled in the counterclockwise sense. Elimination of the t-plane results in an equation directly relating the physical (z) and the computational (w) planes. Three forms of the transformation shown below are equivalent:

$$\frac{dz}{dw} = R \exp\left[\frac{w\pi}{2h}(\phi - \delta)\right] \prod_{j=1}^{j=n} \left[\sinh \frac{\pi}{2h}(w - a_j)\right]^{\alpha_j} \tag{2a}$$

$$= R_1 \exp\left[\frac{w\pi}{2h}(\phi - \delta)\right] \prod_{l=1}^{l=n_1} \left[\sinh \frac{\pi}{2h}(w - a_l)\right]^{\alpha_l}$$

$$\times \prod_{m=1}^{m=n_2} \left[\cosh \frac{\pi}{2h}(w - a_m + ih)\right]^{\alpha_m} \tag{2b}$$

$$= R_2 \exp\left[\frac{w\pi}{2h}(\phi - \delta)\right] \prod_{j=1}^{j=n} \left[\cosh \frac{\pi}{2h}(w - a_j + ih)\right]^{\alpha_j}. \tag{2c}$$

In the above R, R_1, and R_2 are complex constants, a's denote locations of corners in the w-plane, n stands for the total number of corners, n_1 and n_2 denote number of bottom and top corners respectively, subscript l corresponds to the bottom corners and subscript m corresponds to the top corners only, subscript j corresponds to both types of corners, i stands for the imaginary unit $\sqrt{-1}$, and the meanings of the remaining symbols are explained in Fig. 1. The reader may develop a different form of the transformation through the appropriate combination of Eqs. (2a)–(2c).

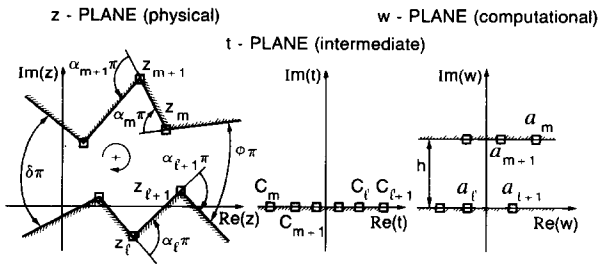

FIG. 1. Mapping of an arbitrary channel into a straight channel.

Davis [3] proposed mapping in the form given by Eq. (2b) and the necessary details for this form of the transformation were worked out by Sridhar and Davis [10]. The form given by Eq. (2a) offers the advantage of the brevity of notation and is used throughout this paper.

The transformation is completed provided locations of the points α in the computational plane, and corresponding to the corners in the physical plane, are known and the complex constant R is determined. This is achieved by applying the numerical procedure described in the next section.

2.1. *Determination of the Parameters of the Transformation*

The difficulties in applying transformation (2) are due to the fact that the relation between a particular channel shape, and the numerical values of the parameters of the appropriate transformation, is not explicit. Therefore, the required parameters have to be determined through a method of successive approximations.

Transformations being considered in this paper are of the Schwarz–Christoffel type [3]. The relation between the z and w planes is given as

$$z = \int_{w_0}^{w} g(w)\, dw + N, \tag{3}$$

where $g(w)$ stands for the right-hand side of Eq. (2). The initial point w_0 in the w-plane can be chosen arbitrarily within the domain $0 \leqslant \mathrm{Im}(w_0) \leqslant h$, $-\infty < \mathrm{Re}(w_0) < +\infty$, and it is taken to be zero throughout this paper. Once the initial point w_0 has been chosen, the constant N controls the location of the channel in the z plane. The constant N is taken to be zero throughout this paper and thus the origins of the z and w planes coincide. If the n turning angles $\alpha_1\pi$, $\alpha_2\pi$,..., $\alpha_n\pi$ are given, the shape of the channel in the z plane is determined uniquely by the choice of n points $a_1, a_2, \ldots, a_n$ in Eq. (2) and is independent of the particular values of the constants w_0 and N in Eq. (3) and R in Eq. (2). The constant R controls the scale of the channel through the value of $|R|$ and its orientation through the value of $\arg(R)$. According to the Riemann's mapping theorem [2], just three of the points a_j may be chosen arbitrarily. The reader should note that the total number of corners in Eq. (2) is $n+2$, where n corners appear explicitly and two degenerate corners enter the equation only implicitly. One of the degenerate corners corresponds to the left end of the channel in the w plane, the origin of the t plane and the left end of the channel in the z plane (Fig. 1). The second degenerate corner corresponds to the right end of the channel in the w plane, $|t| \to \infty$ in the upper t plane and the right end of the channel in the z plane. Therefore, two points belonging to the boundary of the transformed domain are fixed due to the nature of the transformation, and one point remains to be chosen arbitrarily. This choice is accomplished throughout this paper by placing the first bottom corner at the origin of the w plane ($a_1 = 0$). All the remaining parameters are uniquely defined and have to be determined from Eq. (2) as a part of the solution. Sridhar and Davis [10]

argued that the locations of any two corners may be chosen arbitrarily, and, therefore, they predetermined locations of the top and bottom corners farthest to the left in Fig. 1. They also argued that these two corners were to be located one above the other in the w plane. This assumption is correct for configurations with symmetry of the type discussed in Ref. [10]. In problems with no symmetry, Sridhar and Davis [10] considered only channels with a straight section far upstream. The assumption regarding location of the corners is approximately correct, if these two corners are located sufficiently far upstream from the deformed part of the channel. The asymptotic state corresponding to a straight channel upstream is reached exponentially with distance and, therefore, the error of approximation due to the inappropriate selection of the location of the corners decreases exponentially. If the corners are located sufficiently far upstream in the straight section, the error becomes negligible. A solution based on the selection of parameters described in Ref. [10] has been carried out as a test, and it has been found that the type of configurations considered in Ref. [10], together with the method of specification of the shapes of the channel, compensated for the inappropriate selection of the arbitrary parameters. It has, therefore, been concluded that the solution presented by Sridhar and Davis [10] produces correct results only for a limited class of shapes.

The complex constant R and the locations a_j of all the corners, with the exception of the first bottom corner ($a_1 = 0$), have to be determined through a series of successive approximations. The iteration procedure represents an extension of the ideas introduced by Davis [3] and is developed separately for the symmetric and nonsymmetric channels, to take advantage of the considerable simplifications available in the symmetric case.

2.1.1. *Symmetric Channels*

The iteration procedure is simplified by considering only half of the channel (Fig. 2) and making use of the condition of symmetry. Constant R in Eq. (2) can be

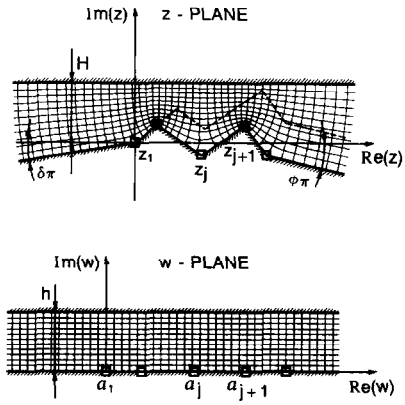

FIG. 2. Mapping of a symmetric channel.

written as $R = |R| \exp(-i\pi\phi)$, where $\phi\pi$ is an angle shown in Fig. 2 and $|R|$ is not known. An initial guess is made for $|R|$ and for locations of corners a_j. The a_j's are picked along the real axis such that $\mathrm{Re}(a_{j-1}) < \mathrm{Re}(a_j) < \mathrm{Re}(a_{j+1})$, where Re denotes a real part. The new value of $|R|$ is adopted by imposing condition,

$$\mathrm{Im}\left[\int_{(0,0)}^{(0,h)} g(w)\, dw\right] = H, \tag{4}$$

where Im denotes an imaginary part, $g(w)$ stands for the right-hand side of Eq. (2), and the remaining symbols are illustrated in Fig. 2. Integration is carried subsequently with the new value of $|R|$ along the bottom of the channel to determine locations of corners in the physical plane. The computed locations do not, in general, coincide with the specified locations. The broken line in Fig. 2 illustrates a typical shape of the channel, corresponding to the assumed locations of corners in the computational plane. The corner turning angles of the computed channel are the same as the turning angles of the specified channel, however, shapes of both channels are not identical due to the difference in distances between the corners. The shapes of both figures can be matched through the appropriate change in the location of corners in the computational plane. The new guess is made for the location of corners by assuming that the a_j's should be rescaled according to the scaling indicated by errors in the distances between the corners in the physical plane

$$\frac{|a_{cj} - a_{c(j-1)}|}{|a_{gj} - a_{g(j-1)}|} = \frac{|z_{cj} - z_{c(j-1)}|}{|z_{gj} - z_{g(j-1)}|}. \tag{5}$$

Here subscript c denotes correct values, g stands for the guessed values, and j denotes corner number. The above procedure is repeated until convergence is achieved. The process converges quite rapidly, even with a poor initial guess. Results for one of the cases considered are displayed in Fig. 2.

2.1.2. *Nonsymmetric Channels*

The case of a nonsymmetric channel is sketched in Fig. 3. The complex constant R in Eq. (2) has the form $R = |R| \exp[i\pi(-\phi_B + \frac{1}{2}\phi_T + \frac{1}{2}\delta_T)]$, where $\phi_B\pi$, $\phi_T\pi$, and $\delta_T\pi$ denote angles shown in Fig. 3 and $|R|$ is not known. The above expression can be verified by letting $w \to \infty$ in Eq. (2). An initial guess is made for $|R|$ and for locations of corners a_j. The a_j's are numbered in the counterclockwise direction starting with a_1 being located at the origin. The initial guess has to be such that $\mathrm{Re}(a_{j-1}) < \mathrm{Re}(a_j) < \mathrm{Re}(a_{j+1})$ along the bottom and $\mathrm{Re}(a_{j-1}) > \mathrm{Re}(a_j) > \mathrm{Re}(a_{j+1})$ along the top, where Re denotes the real part. Bottom corners are located along the real axis and top corners along the axis $w = ih$ (Fig. 3). The new corrected locations of the bottom corners can be evaluated by applying the method described in the previous section. This method requires knowledge of the location of at least one

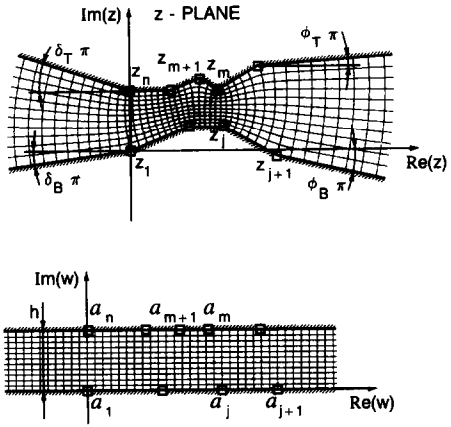

FIG. 3. Mapping of a nonsymmetric channel.

point in the transformed plane and, therefore, it cannot be applied to the top of the channel unless the location of one of the top corners has been predetermined by other means. The top-left corners has been selected for this purpose throughout the paper and its location, together with the new value of $|R|$, is determined by imposing condition

$$\int_{(0,0)}^{a_n} g(w)\, dw = z_n, \tag{6}$$

where $g(w)$ stands for the right-hand side of Eq. (2), subscript n corresponds to the top-left corner, z_n stands for the known location of the top-left corner in the physical plane, and a_n denotes the unknown location of the same corner in the transformed plane. Equation (6) is satisfied provided that the proper values of a_n and $|R|$ have been selected. This is not true in general and, therefore,

$$D(\mathrm{Im}(a_n), |R|) = z_n - z_c \neq 0, \tag{7}$$

where D denotes the difference between the value z_c of the integral on the left-hand side of Eq. (6) and the known value z_n of the right-hand side of Eq. (6). The difference D is a function of $|R|$ and $\mathrm{Re}(a_n)$ only, since it is assumed that the distances between top corners are known. The values of $|R|$ and $\mathrm{Re}(a_n)$ are guessed and the Newton–Raphson procedure is used to correct them until condition $D = 0$ is met with the desired accuracy. This occurs quite rapidly, usually within a couple of iterations. It should be noted that the locations of all top corners vary during the iteration process to keep the distances between the corners unaffected. The location of the bottom-left corner is known and it is assumed that the determined location of

the top-left corner is exact. Now the new a_j's corresponding to the remaining top and bottom corners are determined by applying the method described in the previous section to the top and bottom of the channel. The above procedure is repeated until convergence is achieved. The process converges quite rapidly, even with a poor initial guess. The results are illustrated in Fig. 3.

The iteration procedures described above and in Section 2.1.1 assume that integration of Eq. (2) does not pose any problems. In fact, the required integration can rarely be done analytically and, therefore, a numerical integration has to be introduced to permit applications of transformation (2) to arbitrary shapes.

2.1.3. *Numerical Integration*

The numerical integration of Eq. (2) is complicated due to singularities present when $\alpha_j < 0$. An attempt to integrate this equation across the singularity, by using, say, a midpoint rule, will result in errors due to the nonanalytic nature of the integrand there. The difficulties are avoided by properly adopting integration method described in Ref. [3].

A modified midpoint rule which integrates exactly any nonanalytic term occurring at a corner, is described by examining two adjacent corners, say, k and $k+1$. Equation (2) may be viewed as being made up of three factors on the right-hand side,

$$\frac{dz}{dw} = [F_1(w)\, G_1(w)][F_2(w)\, G_2(w)]\, f(w), \tag{8}$$

where

$$G_1(w) = \left[\frac{\pi}{2h}(w - a_k)\right]^{\alpha_k}; \qquad F_1(w) = \left[\sinh\frac{\pi}{2h}(w - a_k)\right]^{\alpha_k} / G_1(w),$$

$$G_2(w) = \left[\frac{\pi}{2h}(w - a_{k+1})\right]^{\alpha_{k+1}}; \qquad F_2(w) = \left[\sinh\frac{\pi}{2h}(w - a_{k+1})\right]^{\alpha_{k+1}} / G_2(w),$$

and $f(w)$ is a well-behaved function near corners k and $k+1$ resulting from all the remaining corners in the problem. The reader should note that functions F_1 and F_2 are nonsingular and that functions G_1 and G_2 may be singular depending on the sign of α. The integration near k can be carried as

$$z_{m+1} - z_m = \bar{F}_1 \bar{G}_2 \bar{F}_2 f\left[\left(\frac{\pi}{2h}\right)^{\alpha_k} \frac{(w - a_k)^{\alpha_k + 1}}{\alpha_k + 1}\right]_{w_m}^{w_{m+1}}, \tag{9}$$

and near $k+1$,

$$z_{m+1} - z_m = \bar{G}_1 \bar{F}_1 \bar{F}_2 f\left[\left(\frac{\pi}{2h}\right)^{\alpha_{k+1}} \frac{(w - a_{k+1})^{\alpha_{k+1} + 1}}{\alpha_{k+1} + 1}\right]_{w_m}^{w_{m+1}}, \tag{10}$$

where $\bar{F}_1, \bar{F}_2, \bar{G}_1, \bar{G}_2, \bar{f}$ are values of F_1, F_2, G_1, G_2, and f evaluated at $\frac{1}{2}(w_m + w_{m+1})$. Subscript m denotes the integration step. Far away from corners k and $k+1$ both expressions reduce to the midpoint rule,

$$z_{m+1} - z_m = \bar{G}_1 \bar{F}_1 \bar{G}_2 \bar{F}_2 \bar{f} \Delta w. \tag{11}$$

The multiplicative composite formula of the type given in Refs. [3, 13] and valid throughout the whole integration domain, is developed by multiplying the right-hand sides of Eqs. (9) and (10) and dividing by Eq. (11). The general formula, that includes all corners, has the form

$$z_{m+1} - z_m = R \exp\left[\frac{\pi(w_m + w_{m+1})(\phi - \delta)}{4h}\right] (\Delta w)^{1-n} \left(\frac{\pi}{2h}\right)^{\sum_{j=1}^{j=n} \alpha_j} \times \prod_{j=1}^{j=n} \bar{F}_j \left[\frac{(w - a_j)^{\alpha_j + 1}}{\alpha_j + 1}\right]_{w_m}^{w_{m+1}}. \tag{12}$$

Equation (12) correctly accounts for singularities and is of the second-order accuracy type. The testing of the effective accuracy has been done for the sudden expansion of a channel, as shown in Fig. 4. Equation (2) in this particular case has the form

$$\frac{dz}{dw} = \left(\frac{H_2 H_1}{h^2}\right)^{1/2} \left[\sinh \frac{\pi}{2h} w\right]^{1/2} \left[\sinh \frac{\pi}{2h}\left(w - \frac{2h}{\pi} \ln\left(\frac{H_2}{H_1}\right)\right)\right]^{-1/2}. \tag{13}$$

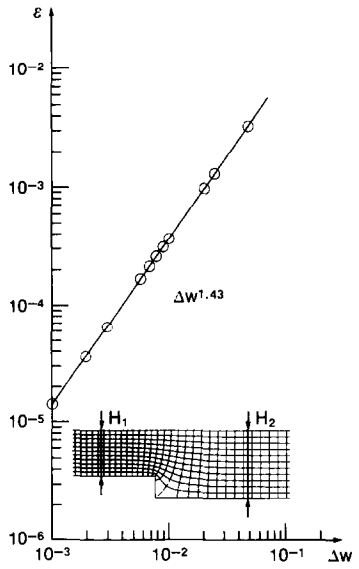

FIG. 4. Accuracy testing of the mapping of a channel bounded by straight-wall elements (Δw — integration step, $\varepsilon = |\hat{h}_c - \hat{h}|$, where $\hat{h}$ stands for the exact value of the metric coefficient and $\hat{h}_c$ denotes the computed value). See text for details.

Analytical integration of the above relation gives

$$z=\frac{H_2}{\pi}\left(\ln\frac{1+s}{1-s}-\frac{H_1}{H_2}\ln\frac{(H_2/H_1)+s}{(H_2/H_1)-s}\right)-i(H_2-H_1), \tag{14}$$

where

$$s^2=\frac{\exp(w\pi/h)-(H_2/H_1)^2}{\exp(w\pi/h)-1}.$$

In the above, h stands for the height of the transformed channel, i is the imaginary unit, and the remaining symbols are explained in Fig. 4. The metric coefficient (Section 4) has been evaluated at $w=(0.1, 0.1)$ by applying the method described in this paper and compared with the exact value given by Eq. (13). The results obtained with the different integration step-sizes are displayed in Fig. 4 and show that the effective accuracy of the method is $\Delta w^{1.43}$.

3. Channel Bounded by Curved Wall Segments

Transformation (2) can be augmented to include channels bounded by curved-wall elements. The augmentation process represents an extension of ideas described in Refs. [3, 14] and is illustrated with the help of the configuration shown in Fig. 5. The curved element is considered as being made up of a large number of straight line segments and the transformation (2a) in the form appropriate for this case can be rewritten as

$$\frac{dz}{dw}=R\exp\left\{\sum_{j=1}^{j=n}\alpha_j\ln\left[\sinh\frac{\pi}{2h}(w-a_j)\right]\right\}. \tag{15}$$

In the limit $n\to\infty$, the straight segment shrinks to zero, the turning angles $\alpha_j\pi$ are replaced by $-\pi d\beta_j$, the locations a_j are replaced by ℓ_j, and the summation in

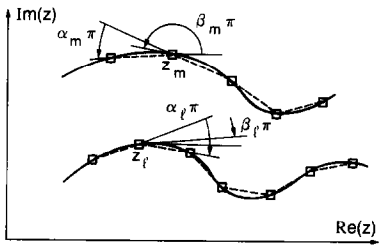

Fig. 5. Mapping of a channel bounded by curved-wall elements.

Eq. (15) is replaced with an integral. Thus, the mapping for a continuous curved element becomes

$$\frac{dz}{dw} = R \exp\left\{-\int \ln\left[\sinh\frac{\pi}{2h}(w-\ell)\right] d\beta\right\}. \tag{16}$$

In the above, ℓ denotes the location of the points belonging to the curved elements in the computational plane and $\pi\beta$ stands for the tangent to the curved element in the physical plane. The minus sign has been added to account for the fact that the turning angles are considered to be positive in the clockwise direction (Section 2) while tangents are positive in the counterclockwise direction. Equation (16) includes Eq. (2), with the exception of the entrance and exit angles. When a corner is encountered, say at a j location, β becomes a step function and the portion of the integral at the corner becomes

$$\int_{\beta_j^-}^{\beta_j^+} \ln\left[\sinh\frac{\pi}{2h}(w-\ell)\right] d\beta = -\alpha_j \ln\left[\sinh\frac{\pi}{2h}(w-a_j)\right], \tag{17}$$

where α_j is the step in β at the location $b = a_j$, i.e., $\alpha_j = \beta_j^- - \beta_j^+$. If the channel is bounded only by straight wall segments, then $d\beta = 0$ except at the corners where $d\beta$ is a step function and the mapping (16) reduces to the form (2a). Equation (16) is, therefore, capable of mapping channels with shapes of a very general nature such as shown, for example, in Fig. 6. The general form of the mapping may be written as

$$\frac{dz}{dw} = R \exp\left[\frac{w\pi}{2h}(\phi-\delta)\right] \exp\left\{\sum_{j=1}^{j=n} \alpha_j \ln\left[\sinh\frac{\pi}{2h}(w-a_j)\right]\right\}$$
$$\times \exp\left\{-\sum_{m=1}^{m=k} \int_{\beta_m}^{\beta_{m+1}} \ln\left[\sinh\frac{\pi}{2h}(w-\ell)\right] d\beta\right\}, \tag{18}$$

where n corners have been extracted and k represents the number of curved segments. The mapping is complete when the locations of corners a_j and curved segments ℓ in the computational plane, corresponding to a given configuration in the physical plane, are established and the complex constant R is known. This may be achieved by applying the numerical procedure described in the next section.

3.1. *Determination of the Parameters of the Transformation*

The angle β appearing in Eq. (18) depends on the geometry of a particular curved-wall segment and is a function of the location along the surface of this segment.

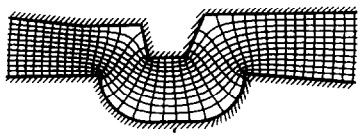

FIG. 6. Mapping of an arbitrary channel.

The curved segments in the transformation (18) may be handled by subdividing them into elements and approximating the β variation on an element with an appropriate analytic function of z. Here it is assumed that the wall shape is analytic on the elements, and therefore care should be taken in making sure that all discontinuities, i.e., corners, curvature discontinuities, etc., appear at the element endpoints.

The shape of a wall element between m and $m+1$ is considered to be analytic and β is approximated as

$$\beta = c_{1m} + c_{2m} \sinh \frac{\pi}{2h}(\ell - \ell_a) + c_{3m} \cosh \frac{\pi}{2h}(\ell - \ell_a), \tag{19}$$

where $\ell_a = \frac{1}{2}(\ell_m + \ell_{m+1})$ denotes location of the middle point of the element in the computational plane and c_{1m}, c_{2m}, and c_{3m} are constants. The integral in Eq. (18) assumes the form

$$\begin{aligned}\int_{\beta_m}^{\beta_{m+1}} \ln\left[\sinh \frac{\pi}{2h}(w-\ell)\right] d\beta &= c_{2m} \frac{\pi}{2h} \int_{\ell_m}^{\ell_{m+1}} \ln\left[\sinh \frac{\pi}{2h}(w-\ell)\right] \cosh \frac{\pi}{2h}(\ell - \ell_a)\, d\ell \\ &\quad + c_{3m} \frac{\pi}{2h} \int_{\ell_m}^{\ell_{m+1}} \ln\left[\sinh \frac{\pi}{2h}(w-\ell)\right] \sinh \frac{\pi}{2h}(\ell - \ell_a)\, d\ell. \end{aligned} \tag{20}$$

The integration in Eq. (20) can be done exactly and the results are expressed as

$$\int_{\beta_m}^{\beta_{m+1}} \ln\left(\sinh \frac{\pi}{2h}(w-\ell)\right] d\beta = c_{2m} \ln g_{2m} + c_{3m} \ln g_{3m}, \tag{21}$$

where

$$g_{2m} = \left[\sinh \frac{\pi}{2h}(w - \ell_{m+1})\right]^{\sinh[(\pi/4h)(\ell_{m+1}-\ell_m)]} \times \left[\sinh \frac{\pi}{2h}(w-\ell_m)\right]^{\sinh[(\pi/4h)(\ell_{m+1}-\ell_m)]} \tag{22}$$

$$\times \left[\frac{\operatorname{ctgh} \frac{\pi}{4h}(w-\ell_{m+1})}{\operatorname{ctgh} \frac{\pi}{4h}(w-\ell_m)}\right]^{\sinh[(\pi/2h)(w-\ell_a)]} \times \exp\left[-2 \sinh \frac{\pi}{4h}(\ell_{m+1} - \ell_m)\right]$$

$$g_{3m} = \left[\frac{\sinh \frac{\pi}{2h}(w-\ell_{m+1})}{\sinh \frac{\pi}{2h}(w-\ell_m)}\right]^{\cosh[(\pi/4h)(\ell_{m+1}-\ell_m)]} \times \left[\frac{\operatorname{ctgh} \frac{\pi}{4h}(w-\ell_{m+1})}{\operatorname{ctgh} \frac{\pi}{4h}(w-\ell_m)}\right]^{\cosh[(\pi/2h)(w-\ell_a)]}. \tag{23}$$

The error introduced by approximation (19) is reduced with reduction of the length of the element. Here, the proper accuracy will be maintained by keeping the length of an element of the same order-of-magnitude as the length of the integration step used for the numerical integration of Eq. (18). One could obviously add higher powers of sinh and cosh in Eq. (19) to improve the accuracy, however, the assumed form, i.e., Eq. (19), is already sufficient to match the assumed surface slope distribution with the correct slopes at m and $m+1$ locations. The numerical integration of Eq. (18) allows one to match the prescribed surface points at the m and $m+1$ locations. Since the element endpoints and slopes are matched with the actual surface, the above formulation has features of a fourth-order method [8]. However, since the integration formula, which will be used in conjunction with Eq. (18), is only $\Delta w^{1.43}$ accurate, the final accuracy is expected to deteriorate.

The general mapping (18), along with the assumed β variation on an element in the form (19), can be rewritten as

$$\frac{dz}{dw} = R \exp\left[\frac{w\pi}{2h}(\phi - \delta)\right] \sum_{m=1}^{m=n} \left[\sinh \frac{\pi}{2h}(w - a_m)\right]^{\alpha_m} g_{2m}^{-c_{2m}} g_{3m}^{-c_{3m}}, \tag{24}$$

where g_{2m} and g_{3m} are given by (22) and (23) and n denotes the number of elements. A corner has been added at the beginning of each element to simplify the notation. The case of $\alpha_m = 0$ corresponds to an element without a corner. Equation (24) can be integrated in the manner described in Section 2.1.3. Each element corresponds to one integration step. Equation (12) is used to handle singularities associated with corners and the contributions due to $g_{2m}^{-c_{2m}}$ and $g_{3m}^{-c_{3m}}$ are obtained by evaluating these terms at the integration step midpoint. Since these terms are nonsingular, the resulting integration has second-order features. The testing of the effective accuracy of the method will be discussed at the end of this section.

The constants in Eq. (19) are to be evaluated from the matching of the assumed surface slope distribution with the surface slope at the element endpoints. This leads to

$$\beta_m = c_{1m} + c_{2m} \sinh \frac{\pi}{2h}(\ell_m - \ell_a) + c_{3m} \cosh \frac{\pi}{2h}(\ell_m - \ell_a), \tag{25}$$

$$\beta_{m+1} = c_{1m} + c_{2m} \sinh \frac{\pi}{2h}(\ell_{m+1} - \ell_a) + c_{3m} \cosh \frac{\pi}{2h}(\ell_{m+1} - \ell_a), \tag{26}$$

where β_m and β_{m+1} are known. The third equation is obtained by properly interpreting the numerical integration formula. Since the midpoint rule is employed, the curved element is replaced during the integration process by a straight element, whose slope θ_m is given by

$$\theta_m = c_{1m} + c_{2m}. \tag{27}$$

This equation comes from (19) and can be verified by evaluating the change of the argument on an element in Eq. (24). The midpoint rule is equivalent to the

trapezoidal rule for well-behaved functions [15], and the slope θ_m is the same as the tangent to the straight line connecting points m and $m+1$. The angle θ_m is, therefore, considered to be a known quantity and is used in evaluation of the constants c_{1m}, c_{2m}, and c_{3m}. Elimination of the unknowns from Eqs. (25)–(27) results in

$$c_{1m} = \theta_m - \left(\theta_m - \frac{1}{2}(\beta_{m+1} + \beta_m)\right) \Big/ \left(1 - \cosh\frac{\pi}{4h}(\ell_{m+1} - \ell_m)\right), \tag{28}$$

$$c_{2m} = (\beta_{m+1} - \beta_m)/2 \sinh\frac{\pi}{4h}(\ell_{m+1} - \ell_m), \tag{29}$$

$$c_{3m} = \left(\theta_m - \frac{1}{2}(\beta_{m-1} + \beta_m)\right) \Big/ \left(1 - \cosh\frac{\pi}{4h}(\ell_{m+1} - \ell_m)\right). \tag{30}$$

The last equation is rewritten as

$$\theta_m = \frac{1}{2}(\beta_{m+1} + \beta_m) + c_{3m}\left[1 - \cosh\frac{\pi}{4h}(\ell_{m+1} - \ell_m)\right] \tag{31}$$

to demonstrate that the slope of the straight line connecting points m and $m+1$ is not equal to the average angle on the element, as it might be expected from a numerical integration. The quantity c_{3m} may be viewed as an angle correction factor ensuring that after the mapping the angular rotation will be exactly as specified by Eq. (11). The reader should note that the transformation (24) requires only the knowledge of c_{2m} and c_{3m} and the evaluation of c_{1m} is not required.

The location of the element endpoints ℓ_m in the computational plane, corresponding to their known locations z_m in the physical plane, have to be established through a method of successive approximations. The procedure is exactly the same as described in Section 2.1. The ℓ_m's are guessed initially and are iteratively corrected by Eq. (5), where the a_{cj} and a_{gj} are replaced with ℓ_{cj} and ℓ_{gj}. Similarly, $|R|$ is established through the iterations, while $\arg(R)$ assumes the values given in Sections 2.1.1 and 2.1.2. The process converges as rapidly as in the case of a channel bounded by the straight wall segments. The testing of the accuracy has been done for the channel shown in Fig. 7. The exact transformation has the form

$$w = Az + B\tanh\frac{\pi}{2}z, \tag{32}$$

where the values $A = 0.5$ and $B = 0.2$ have been selected. The upper wall of the channel is described by the line corresponding to $\mathrm{Im}(w) = 0.485$. The same channel has been mapped using the method described earlier in this section, the metric coefficient (Section 4) has been evaluated at $w = (0.1, 0.4365)$ and compared with its exact value. The results are displayed in Fig. 7 and show that the effective accuracy of the method is $\Delta w^{3.49}$.

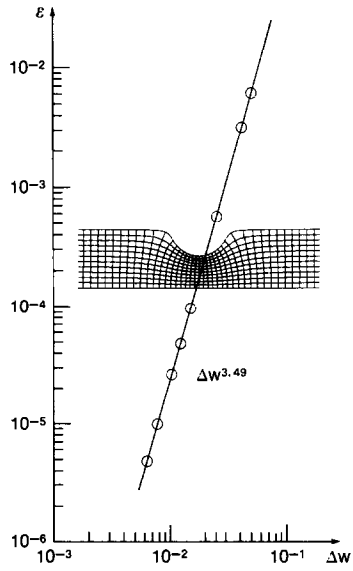

FIG. 7. Accuracy testing of the mapping of a channel bounded by curved-wall elements (Δw – integration step, $\varepsilon = |\hat{h}_c - \hat{h}|$, where $\hat{h}$ stands for the exact value of the metric coefficient and $\hat{h}_c$ denotes the computed value). See text for details.

4. METRIC COEFFICIENTS

Transformations described in this paper may be used to generate several different coordinate systems, which may be conformal or nonconformal, orthogonal or non-orthogonal. This section provides only a description of the simplest systems. The reader may consult Refs. [4, 10, 11, 12] to get an overview of the potentials of the method based on conformal transformations.

The simplest coordinate system is defined by lines $\xi = \text{const.}$ and $\eta = \text{const.}$ in the computational plane ($w = \xi + i\eta$). The metric coefficients which define the ratio of the differential distances in the $z = x + iy$ plane to the differentials of the coordinate parameters in the $w = \xi + i\eta$ plane, have the form

$$\hat{h}_\xi = \left[\left(\frac{\partial x}{\partial \xi}\right)^2 + \left(\frac{\partial y}{\partial \xi}\right)^2\right]^{1/2} \qquad \hat{h}_\eta = \left[\left(\frac{\partial x}{\partial \eta}\right)^2 + \left(\frac{\partial y}{\partial \eta}\right)^2\right]^{1/2}. \tag{33}$$

It can be shown that in the case of a conformal mapping

$$\hat{h}_\xi = \hat{h}_\eta = \hat{h} = \left|\frac{dz}{dw}\right| \tag{34}$$

and the coordinate system is characterized by only one metric coefficient, which can be easily determined from Eq. (2) or (18).

Coordinates suitable for axisymmetric channel can be constructed through the rotation of a two-dimensional system around the appropriate axis (rotation around the top of the configuration displayed in Fig. 2). The metric coefficient corresponding to the angular rotation, is equal to the distance from the axis of rotation and may be obtained through the integration of Eq. (2) or (18).

A certain class of three-dimensional coordinate systems may be obtained through an appropriate translation of the two-dimensional systems, such as described in this paper, in the third direction. A trivial example is provided by considering the third dimension to be Cartesian. Another class of the three-dimensional configurations may be considered by noting that the conformal mapping provides a surface-to-surface correspondence that is not limited only to the planar surfaces [4, 9].

5. Potential Flow

The determination of the parameters of transformations (2) and (18) is equivalent to the solution of the Laplace equation and may be conveniently interpreted as a solution of the potential flow problem in a channel. The complex potential, $\Omega = \Phi + i\Psi$, in the transformed plane has the form

$$\Omega = Aw. \tag{35}$$

The complex velocity at a point in the physical plane is given by

$$u - iv = \frac{d\Omega}{dz} = \frac{d\Omega}{dw}\Big/\frac{dz}{dw} = A\Big/\frac{dz}{dw}. \tag{36}$$

The constant A may be determined from the known flow condition. In the case of a straight channel upstream, $u \to U_1$ as $w \to -\infty$, and $A = U_1 H_1/h$, where H_1 is the distance between the walls far upstream in the physical plane. When the channel is straight downstream, $u \to U_2$ as $w \to +\infty$ and $A = U_2 H_2/h$, where H_2 is the spacing between the walls far downstream. Straight channel upstream and downstream corresponds to $A = RU_1(H_1/H_2)^{1/2} = RU_2(H_2/H_1)^{1/2}$. When the flow rate Q is given, $A = Q/h$.

Pressure field can be easily specified in terms of the pressure coefficient

$$C_p = \frac{p - p_0}{\frac{1}{2}\rho U_0^2} = 1 - \frac{A^2}{U_0^2 \hat{h}^2}, \tag{37}$$

where p_0 and U_0 are pressure and velocity at a reference point and $\hat{h}$ is given by Eq. (34).

6. Concluding Remarks

A coordinate generation method for channel flows has been developed. The method involves conformal mapping of the channel of an arbitrary shape in the physical plane into a straight channel in the computational plane. The mapping, which is given explicitly, involves parameters defined in the computational plane and thus not known a priori for the specified configuration in the physical plane. A method of successive approximations, leading to the determination of the required parameters, is presented. The method is $\Delta w^{1.43}$ accurate in the case of channels bounded by straight-wall elements and $\Delta w^{3.49}$ accurate in the case of channels bounded by curved-wall elements; it has a very simple logic, is easy to program, and converges quite rapidly. Several configurations of a rather extreme geometry and involving up to three hundred points have been solved without encountering difficulties. As a byproduct the method produces a solution of the potential flow problem for the given configuration.

References

1. O. L. Anderson, R. T. Davis, G. B. Hankins, and D. E. Edwards, Solution of viscous internal flows on curvilinear grids generated by the Schwarz–Christoffel transformation, *in* "Numerical Grid Generation" (J. F. Thompson, Ed.), North-Holland, Amsterdam, 1982.
2. G. F. Carrier, M. Krook, and C. E. Pearson, "Functions of a Complex Variable," McGraw–Hill, New York, 1966.
3. R. T. Davis, "Numerical Methods for Coordinate Generation Based on the Schwarz–Christoffel Transformation," AIAA Paper No. 79–1463, 4th Computational Fluid Dynamics Conference, 1979.
4. D. C. Ives, Conformal grid generation, *in* "Numerical Grid Generation" (J. F. Thompson, Ed.), North-Holland, Amsterdam, 1982.
5. D. D. Knight, Application of curvilinear coordinate gneration techniques to the computation of internal flows, *in* "Numerical Grid Generation" (J. F. Thompson, Ed.), North-Holland, Amsterdam, 1982.
6. H. Kober, "Dictionary of Conformal Representations," Dover, New York, 1952.
7. V. O'Brien, *J. Comput. Phys.* **44** (1981), 220.
8. R. Peyret and T. D. Taylor, "Computational Methods for Fluid Flows," Springer-Verlag, Berlin, 1983.
9. A. V. Pogorelov, "Differential Geometry," Noordhoff, Groningen, 1959.
10. K. P. Sridhar and R. T. Davis, A Schwarz–Christoffel method for generating internal flow grids, *in* "Computers in Flow Predictions and Fluid Dynamics Experiments" (K. N. Ghia, T. S. Mueller, and B. R. Patel, Eds.), ASME Winter Annual Meeting, Washington, D.C., 1981.
11. J. F. Thompson, "A Survey of Grid Generation Techniques in Computational Fluid Dynamics," AIAA Paper No. 83-0447, AIAA 21st Aerospace Sciences Meeting, 1983.
12. J. F. Thompson and Z. U. A. Warsi, *J. Comput. Phys.* **47** (1982), 1.
13. M. Van Dyke, "Perturbation Methods in Fluid Dynamics," Parabolic Press, 1975.
14. L. C. Woods, "The Theory of Subsonic Plane Flow," Cambridge Univ. Press, London/New York, 1961.
15. D. M. Young and R. T. Gregory, "A Survey of Numerical Mathematics," Addison–Wesley, Reading, Mass., 1973.